Pergamon

Int. J. Heat Mass Transfer. Vol. 37, No. 17, pp. 2707–2714, 1994

0017–9310/94 $7.00 + 0.00

0017–9310(94)E0095–C

Mainstream turbulence effect on film effectiveness and heat transfer coefficient of a gas turbine blade with air and CO_2 film injection

ANANT B. MEHENDALE, SRINATH V. EKKAD and JE-CHIN HAN

Turbine Heat Transfer Laboratory, Department of Mechanical Engineering, Texas A&M University, College Station, TX 77843-3123, U.S.A.

(*Received* 27 *August* 1993 *and in final form* 28 *February* 1994)

Abstract—Effect of grid-generated mainstream turbulence on the film effectiveness and heat transfer coefficient of a turbine blade model was investigated at a chord Reynolds number of 3×10^5. The blade model had three rows of film holes in the leading edge region and two rows each on the pressure and suction surfaces. CO_2 and air, with density ratios (DRs) of about 1.5 and 1.0, respectively, were used as film injectants. Results indicate that an increase in mainstream turbulence causes an increase in Nusselt numbers and a decrease in film effectiveness, over most of the blade surface, for both density ratio injectants at all blowing ratios.

INTRODUCTION

IT IS well known that gas turbine performance improves with an increase in turbine inlet temperature. This has caused a continuing trend towards higher gas turbine inlet temperatures and has resulted in higher heat loads on turbine components. Hence, sophisticated turbine blade cooling techniques must be employed in order to maintain the peformance requirements.

There have been many investigations to study the effect of film injection on flat or curved surfaces at low mainstream turbulence intensities. The effects of blowing ratio, injection geometry, and film coolant have been investigated by Goldstein [1], Han and Mehendale [2], and Schwarz *et al.* [3].

Mick and Mayle [4] studied heat transfer coefficient and film effectiveness distributions for a low mainstream turbulence flow on a leading edge model. Mehendale and Han [5, 6] studied the effect of high mainstream turbulence and film hole spacing on film effectiveness and heat transfer coefficient from a leading edge model. They reported that an increase in mainstream turbulence causes an increase in heat transfer coefficient and a decrease in film effectiveness.

The effect of secondary-to-mainstream density ratio for film injection on a flat plate has been studied by Goldstein *et al.* [7], Pedersen *et al.* [8], and Sinha *et al.* [9]. Most of these studies were performed at low mainstream turbulence intensities. They reported higher film effectiveness for higher density injectant. Teekaram *et al.* [10] reported that film-cooled heat transfer coefficients were independent of the injectant (air or CO_2) as long as their densities were maintained the same.

Abhari and Epstein [11] studied heat transfer on a film cooled rotor blade, under simulated non-dimensional engine conditions, with time resolved measurements. They reported that film cooling reduced the time-averaged heat transfer by as much as 60% on the suction surface, but the effect was relatively little on the pressure surface. Takeishi *et al.* [12] compared film effectiveness for a stationary cascade under 4% mainstream turbulence intensity and for a rotor blade using the heat–mass transfer analogy. They reported that in the leading-edge region and on the suction surface, film effectiveness for the cascade and rotor blade match well, but the cascade values are higher on the pressure surface. Ou *et al.* [13] and Mehendale *et al.* [14] studied the effects of incident unsteady wake conditions (to simulate unsteady wakes shed by rotor blades) and secondary-to-mainstream density ratio (1.0 and 1.5) on blade heat transfer coefficient and film effectiveness from a linear turbine blade cascade. They reported that an increase in unsteady wake strength causes an increase in heat transfer coefficient and a decrease in film effectiveness. They also reported that higher density ratio injectant provides better film effectiveness at higher blowing ratios.

This study focuses on the effect of grid-generated mainstream turbulence (to simulate turbulence at combustor outlet) on the heat transfer coefficient and film effectiveness distributions of a turbine blade

NOMENCLATURE

C	blade chord	Re	cascade inlet Reynolds number based on the blade chord, $V_1 C/\nu$
D	film hole diameter	T_{aw}	local adiabatic wall temperature
DR	density ratio (secondary to mainstream), ρ_s/ρ_∞	T_s	secondary flow temperature within injection cavity
h	local heat transfer coefficient	T_w	local wall temperature
I	momentum flux ratio (secondary to mainstream), $(\rho V^2)_s/(\rho V^2)_\infty$	T_∞	mainstream temperature at cascade inlet
k	local air thermal conductivity	V	local mainstream velocity
M	blowing ratio (secondary to mainstream mass flow ratio), $(\rho V)_s/(\rho V)_\infty$	V_1	mean mainstream velocity at cascade inlet
Nu	local Nusselt number based on blade chord, hC/k	X	streamwise distance from stagnation along blade surface.
$\overline{Nu}$	spanwise-averaged Nusselt number		
P	film hole pitch		
q''_{cond}	local conduction heat loss flux	Greek symbols	
$q''_{cond,g}$	local conduction heat gain flux	η	local film effectiveness
q''_{gen}	foil generated wall heat flux	$\bar{\eta}$	spanwise-averaged film effectiveness
q''_{rad}	local radiation heat loss flux	ν	kinematic viscosity.

model with air (DR $\approx$ 1.0) or CO_2 (DR $\approx$ 1.5) film injection through three rows of film holes in the leading edge region and two rows each on the pressure and suction surfaces. The effect of grid-generated mainstream turbulence on the blade heat transfer coefficient was also studied on an identical-profile blade model for fundamental understanding and comparison purposes.

The objectives of this study are to determine: (1) enhancement in blade heat transfer coefficients only due to mainstream turbulence (i.e. for the no-film-holes blade model); (2) enhancement in blade heat transfer coefficients only due to film holes (i.e. for the blade model with film holes, but without film injection) for the no-grid condition; (3) enhancement in blade heat transfer coefficients only due to film injection (i.e. for the no-grid condition); (4) the effect of blowing ratio (air or CO_2 film injection) on blade heat transfer coefficient and film effectiveness; (5) the effect of injectant density on blade heat transfer coefficient and film effectivenesss with air or CO_2 film injection; and (6) the combined effect of mainstream turbulence and injectant density on blade heat transfer coefficient and film effectiveness.

TEST APPARATUS AND INSTRUMENTATION

A schematic of the test apparatus is shown in Fig. 1(a). The test apparatus consisted of a low speed, low turbulence wind tunnel with an inlet nozzle, a turbulence grid, a linear turbine blade cascade with an instrumented blade at its center, and a suction type blower. The wind tunnel was dsigned for a blade turning angle of 107.49°. The five blade cascade was installed downstream of the turbulence grid.

A detailed view of the cascade is shown in Fig. 1(b). The cascade was designed for use in our low speed wind tunnel test facility. The blade and cascade configuration was designed to produce a similar velocity ratio distribution as in a typical advanced high pres-

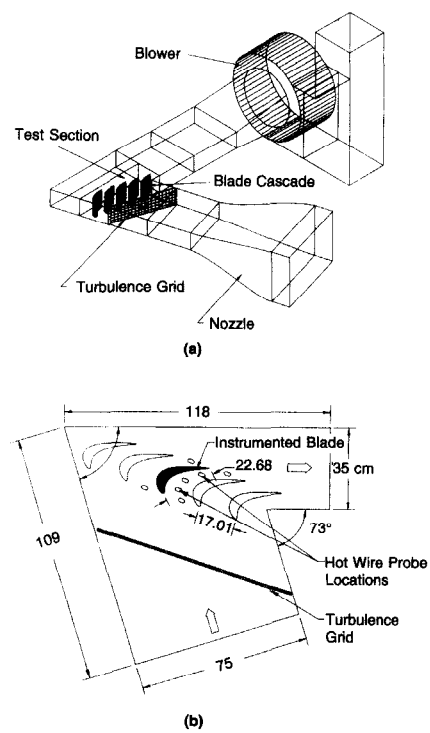

FIG. 1. (a) Schematic of the linear turbine blade cascade with a turbulence grid. (b) Cascade geometry and instrumentation location layout.

sure turbine blade row. The selected blade had a 107.49° turning with relative flow angles of 35° and −72.49° at the blade inlet and exit, respectively. A five-times scaled up model was used to simulate the engine Reynolds number. The cascade had five blades, each with a chord length of 22.68 cm and a radial span of 25.2 cm. The blades were spaced 17.01 cm apart at the cascade inlet. All blades were made of high quality model wood. Only the center blade was instrumented and was either the blade without film holes or the blade with film holes.

The turbulence grid was made of 1.3 cm square brass tubes spaced 4.8 cm apart in both horizontal and vertical directions. The turbulence grid was located 21, 30, or 60 cm upstream of the cascade leading edge, depending on the desired turbulence intensity. The locations correspond to 16.5, 23.6, or 47.3 tube widths, respectively.

As shown in Fig. 1(b), slots were machined in the top wall of the wind tunnel for inserting flow measurement probes. Hot wire probes were inserted through the leading edge slots to measure the oncoming flow velocity, turbulent fluctuations, and to check the flow periodicity between the adjacent flow passages. The exit flow velocities were measured through the trailing edge slots. Instantaneous velocity fluctuations at locations in the flow passages were measured through the remaining slots.

A calibrated, single hot wire probe was used to measure mainstream flow behavior. It was connected to a four-channel TSI IFA · 100 hot wire anemometer. The analog signal was digitized by a Data Translation 250 kHz A/D board in a 386SX 20 MHz machine.

Twenty-six strips of stainless steel foil, each 25.4 cm long, 1.8 cm wide and 0.00378 cm thick, were cemented vertically on the test blade without film holes. The foils were separated by 0.8 mm gaps that were filled with wood putty and made flush with the foil surface. All foils were connected in series by copper bus bars. The foils produced an almost constant wall heat flux boundary condition when electrically heated. Thirty-six gage copper–constantan thermocouples were cemented on the undersides of the foils. There were 11 rows of thermocouples on the pressure surface and 15 rows on the suction surface. Each row had 3 thermocouples spaced 2.52 cm apart in the radial midspan region of the blade.

A schematic of the top view of the blade with film holes is shown in Fig. 2. The first cavity supplied three rows of film holes—one near the leading edge, and one each on the pressure and suction surfaces. The second cavity supplied one row each on the pressure and suction surfaces. The third and fourth cavities supplied one row of film holes on the pressure and suction surfaces, respectively. Depending on its location, each row had 8 to 10 film holes between 30% and 70% of the radial blade span. Some of the film holes had a compound angle (radial and tangential) relative to the blade surface as seen in the figure. (Radial angle is defined as the angle between the film hole axis and the local radial (spanwise) direction. Tangential angle is defined as the angle between the film hole axis and the local streamwise tangential direction.) Details of the film hole configuration (streamwise location, diameter, length, spanwise spacing, and compound angle) for this 5X model blade were specified by General Electric, Aircraft Engine Division. Each cavity was connected with individually controllable injectant (air or CO_2) supply lines. Similar to the blade without film holes, this blade was instrumented with thin foils and thermocouples except that foils did not cover the film hole regions. Thirty-six gage copper–constantan thermocouples were cemented on the undersides of the foils. There were 9 rows of thermocouples on the pressure surface and 13 rows on the suction surface. Each thermocouple row had 4 thermocoules placed at strategic locations in the radial midspan region. Thermocouples were mounted within the injection cavities to measure the secondary flow temperatures just before injection. All thermocouples were connected to a 100 channel Fluke 2280A datalogger interfaced with the 386SX machine. Input voltage and line current for both test blades were measured with a Fluke multimeter and a current clamp.

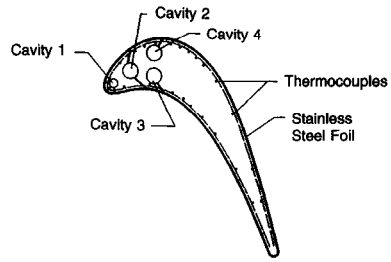

Film Hole Row Location	P/D	Axial Angle	Radial Angle	Tangential Angle
Cavity 1: All Three	7.31	90°	27°	–
Cavity 2: Pressure Side	6.79	–	32°	55°
Cavity 2: Suction Side	4.13	–	90°	45°
Cavity 3: Pressure Side	5.00	–	35°	50°
Cavity 4: Suction Side	5.71	–	90°	30°

FIG. 2. Schematic of the blade with film holes.

TEST CONDITIONS AND DATA ANALYSIS

All tests were performed at the chord Reynolds number (Re) of 3×10^5. This corresponds to an inlet velocity of 21 m s^{-1}. The cascade outlet velocity was 50 m s^{-1}. Four turbulence conditions at the cascade inlet were studied: (1) the no turbulence grid condition ($Tu = 0.7\%$); (2) the low mainstream turbulence condition ($Tu = 5\%$); (3) the medium mainstream turbulence condition ($Tu = 13.4\%$); and (4) the high mainsteam turbulence condition ($Tu = 17\%$).

For the blade with film holes, the secondary (injectant) mass flux rate for a given row of injection holes

was based on the local mainstream velocity (V) at that location (as measured with a pressure tap instrumented blade, see Han *et al.* [15]) and the desired blowing ratio. Tests were conducted at the blowing ratios of 0.4, 0.8 and 1.2. During the heat transfer coefficient tests, the stainless steel foils were electrically heated and the injectant (air or CO_2) temperature was maintained the same as the ambient mainstream temperature; whereas, during the film effectiveness tests, no foil heat was applied and the injectant (air or CO_2) was heated.

As in Mehendale and Han [6] and Ou *et al.* [13], the local heat transfer coefficient with or without film injection was calculated from

$$h = \frac{q''_{\text{gen}} - (q''_{\text{cond}} - q''_{\text{rad}})}{T_w - T_\infty} = \frac{q''_{\text{gen}} - (q''_{\text{cond}} - q''_{\text{rad}})}{T_w - T_{aw}} \quad (1)$$

since Mach number $\ll 1$.

During the heat transfer coefficient tests, T_w was in the 40–50°C range and T_{aw} was about 25°C. Heat loss tests were performed to estimate the total heat loss. The measured total heat loss was about 10% of the foil generated heat. The conduction and radiation heat losses were 4% and 6%, respectively, of the heat generated. Heat loss through the tiny thermocouple wires was estimated to be very small (less than 0.1%), and axial and lateral conduction through the thin foil was also found to be negligible.

The local Nusselt number (Nu) was calculated from $Nu = hC/k$, where h is the local heat transfer coefficient, C is the blade chord length, and k is the local thermal conductivity. Local Nusselt numbers at a given streamwise location were averaged to obtain the spanwise-averaged Nusselt number ($\overline{Nu}$) at that location.

As in Mehendale and Han [6] and Mehendale *et al.* [14], local film effectiveness was calculated from

$$\eta = \frac{T_w - T_\infty}{T_s - T_\infty} + \frac{(q''_{\text{cond}} + q''_{\text{rad}}) - q''_{\text{cond,g}}}{h(T_s - T_\infty)}. \quad (2)$$

During the film effectiveness tests, T_s was maintained at about 50°C. Local film effectiveness values at a given streamwise location were averaged to obtain the spanwise-averaged film effectivenesss ($\bar{\eta}$) at that location.

The above-mentioned thin foil-thermocouple technique and the related data analysis method to calculate the heat transfer coefficient and film effectiveness are the same as in Mehendale and Han [5, 6]. An uncertainty analysis as in Kline and McClintock [16] showed the uncertainty in Nusselt number and film effectivenesss to be $\pm 5\%$ based on 20:1 odds.

RESULTS AND DISCUSSION

Velocity profiles at the inlet and outlet of the left and right flow paths were recorded in the spanwise direction. The dimensionless velocity profiles at the inlet and outlet of the flow paths are shown in Ou *et al.* [13]. Results indicate that the inlet and outlet velocity profiles in the flow paths are essentially uniform in the 50% midspan region. Also, the flow direction at the inlet and outlet of both flow paths was uniform. Thus, the Nusselt numbers are free from the top and bottom wall boundary layer effects. An identical profile blade with static pressure taps was used to measure the local mainstream velocity distribution around the blade (Han *et al.* [15]). The distribution of local-to-exit velocity ratio (V/V_2) is shown in Ou *et al.* [13]. The results indicate that the suction side velocity is higher than the pressure side velocity.

The effect of mainstream turbulence on spanwise averaged Nusselt number distribution for the blade without film holes is shown in Fig. 3. Results for the no-grid base condition show that Nusselt number on the suction surface decreases gradually with increasing streamwise distance from stagnation due to laminar boundary layer growth; but past $X/C = 0.85$ (i.e. 85% chord), the Nusselt number increases sharply due to boundary layer transition. For the same no-grid condition, the Nusselt number on the pressure surface decreases sharply with increasing X/C (due to a much lower flow velocity and hence a faster boundary layer growth), but starts to increase from $X/C = -0.2$ due to a strong acceleration. As mainstream turbulence increases, the increased flow fluctuations disturb the boundary layer and cause an increase in the heat transfer coefficient distribution over the entire blade surface. This effect is more severe on the suction surface than on the pressure surface. The upstream flow fluctuations cause an earlier laminar-to-turbulent boundary layer transition on the suction surface (at only half the distance as for the no-grid case) and the transition length increases (due to a strong acceleration in the mid-chord region which delays the production of turbulence spots) with increasing mainstream turbulence. The increases in heat transfer coefficients from the no-grid case ($Tu = 0.7\%$) to $Tu = 17\%$ vary from 19% near the leading edge to as high as 239% at $X/C = 0.85$ on the suction surface; whereas the increases vary from 31%

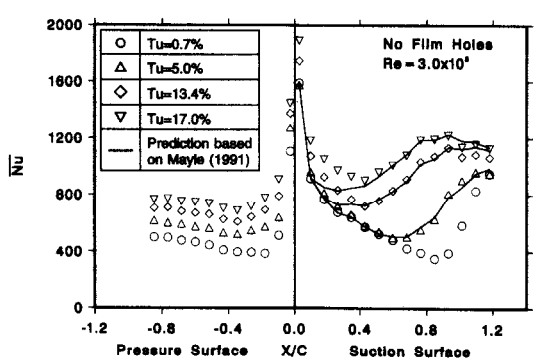

FIG. 3. Effect of mainstream turbulence on $\overline{Nu}$ distribution for the blade without film holes.

near the leading edge to 101% at $X/C = -0.2$ on the pressure surface.

Also shown in Fig. 3 are the present predictions of transition, induced by grid-generated mainstream turbulence, based on the intermittency transition theory of Mayle [17]. He suggested that the boundary layer transition from laminar to turbulent flow on blade suction surface is composed of two parts: bypass transition and unsteady wake induced transition. His theory predicts the present data reasonably well, except in the region before transition at high turbulence levels, where it underpredicts the data, as seen from the figure.

The effect of only film holes (i.e. without film injection) on spanwise-averaged Nusselt number distribution is shown in Fig. 4. It can be seen very clearly that just the film holes can cause significant increases in heat transfer coefficients. This may be because the leading edge film holes disturb the boundary layer considerably and this highly disturbed boundary layer is further tripped by the subsequent film holes, which results in high heat transfer coefficients. The increases are as high as 235% and 153% on the pressure and suction surface, respectively. Over almost half of the suction surface, heat transfer coefficients for this case are comparable with even the 'strongest turbulence ($Tu = 17\%$) and no film holes' case.

With film injection (Fig. 4), the sharp increases in heat transfer coefficients immediately downstream of the film hole row locations on the suction surface are caused by the highly disturbed boundary layer due to the injectant–mainstream interaction. Following such peaks, boundary layer growth and stabilization cause the heat transfer coefficients to decrase. Since a lower mainstream velocity produces a thicker boundary layer on the pressure surface than on the suction surface, increases in heat transfer coefficients by flow disturbances due to film injection are less prominent on the pressure surface. As seen, just film injection by itself can enhance heat transfer coefficients over the no-film-holes case by as much as 59% and 201% on the pressure and suction sides, respectively. An increase in blowing ratio causes an increased injectant–mainstream interaction and results in an increase in heat transfer coefficients over the blade surface for both density injectants as shown in Fig. 4. The effect of blowing ratio decreases farther downstream of the last row of film holes due to boundary layer stabilization.

For a given blowing ratio, as the density ratio increases, the momentum flux ratio decreases. Hence, at the same blowing ratio, the lower density injectant jet (air, DR = 1.0) penetrates further than the higher density injectant jet (CO_2, DR = 1.52). This causes a higher jet–mainstream interaction for the lower density ratio injectant and results in higher heat transfer coefficients. The effect of density ratio is more pronounced just downstream of most of the film holes, where heat tansfer coefficients for air injection are higher than for CO_2 injection as shown in Fig. 4. Downstream of the second row of film holes on the suction surface, the higher density ratio injectant (CO_2) produces higher heat transfer coefficients. This may be because the lower momentum flux ratio CO_2 injection stays closer to the blade, causes an accumulation effect, and thus produces an earlier transition to the turbulent boundary layer.

The effect of film injection on spanwise-averaged film effectiveness distribution for air (DR = 0.97) or CO_2 (DR = 1.48) injection is shown in Fig. 5. These figures show only the effect of film injection, i.e. for the no-grid condition. In general, film effectiveness increases downstream of film holes for both air and CO_2 injections. These peaks in film effectiveness are due to better film coverage downstream of film holes. Following such peaks, film effectiveness decreases due

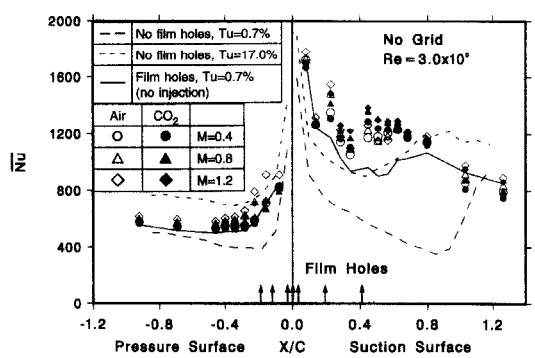

FIG. 4. Effect of air or CO_2 injection on $\overline{Nu}$ distributions for the no-grid case.

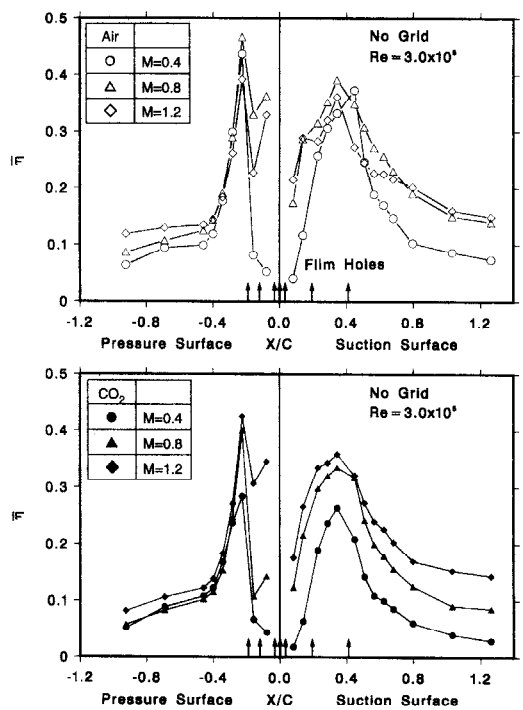

FIG. 5. Effect of air or CO_2 injection on $\bar{\eta}$ disributions for the no-grid case.

to injectant dilution and the values are very small far downstream of the film holes. For air injection, the blowing ratio of 0.8 (with a medium momentum flux ratio and a medium mass flow rate) provides optimum film coverage and hence the best film effectiveness over most of the blade surface. At the higher blowing ratio of 1.2, a significantly higher momentum flux ratio causes more injectant jet penetration into the mainstream which results in lower film effectivness. At the lower blowing ratio of 0.4, only a small amount of injectant comes out of the film holes, which results in lower film effectiveness. For CO_2 injection, the blowing ratio of 1.2 provides the best film effectivness over most of the blade surface. Since CO_2 is about 1.5 times as dense as air, its momentum flux ratio at the blowing ratio of 1.2 is only 66% that of air injection at the same blowing ratio, which results in a lesser jet penetration. This lesser jet penetration combined with the highest injectant mass flow rate at this blowing ratio results in the best film coverage.

At the lowest blowing ratio of 0.4, film effectiveness values near the leading edge are very small but they increase further downstream and subsequently decrease due to film dilution. Since local mainstream velocities near the leading edge are very small, a very small amount of injectant comes out at the lowest blowing ratio of 0.4. Hence, it produces lower film effectiveness near the leading edge. However, since its momentum flux ratio is small, the injectant at the blowing ratio of 0.4 gets trapped in the boundary layer. This effect accumulates with injections from the downstream rows and increases film effectiveness. Farther downstream of the last row of film holes, even the blowing ratio of 1.2 (i.e. even with much higher penetration into the mainstream) shows higher film effectiveness than the blowing ratio of 0.4, due to jet spreading which causes the jet to come in contact with the far downstream surface and also due to higher injectant mass.

The effect of mainstream turbulence on spanwise-averaged Nusselt number distribution for air or CO_2 injection at the blowing ratios of 0.4, 0.8 and 1.2 is shown in Figs. 6, 7 and 8, respectively. The mainstream turbulence effect in addition to the film injection effect is shown in these figures. As mainstream turbulence increases, unsteady flow fluctuations disturb the boundary layer and cause higher heat transfer coefficients at all locations for both injectants at all blowing ratios. As blowing ratio increases, the jet–mainstream interaction induced boundary layer disturbance increases. Under such highly disturbed boundary layer conditions at higher blowing ratios, further effect of mainstream turbulence (from 0.7% to 17%) is not as significant as under less disturbed boundary layer conditions as at lower blowing ratios. Thus, as blowing ratio increases, the increases in heat transfer coefficients due to mainstream turbulence (from $Tu = 0.7\%$ to $Tu = 17\%$) reduce for both density ratio injectants. This behavior is observed over most of the blade surface except in the accumulation

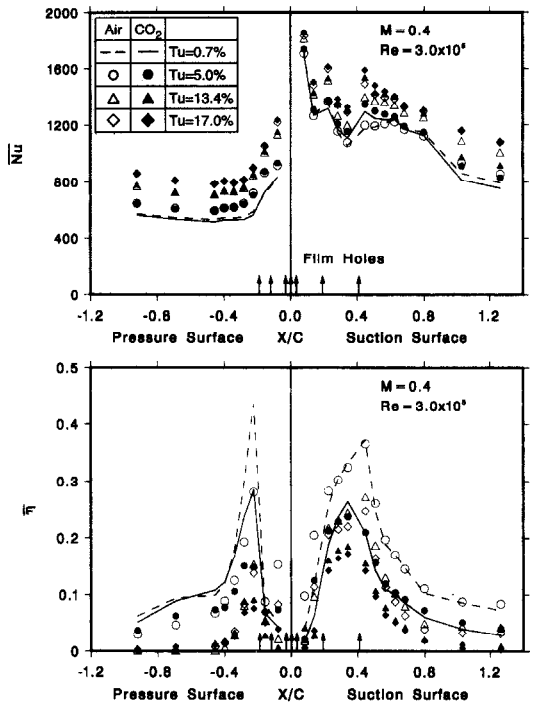

FIG. 6. Effect of mainstream turbulence and air or CO_2 injection on $\overline{Nu}$ and $\bar{\eta}$ distributions for $M = 0.4$.

effect region on the suction surface ($X/C > 0.4$) where it is reversed. The reason for this reversed behavior in the accumulation region is because, at higher blowing ratios, there is a lesser amount of accumulation in the boundary layer due to higher jet penetration into the mainstream. Hence, in the accumulation region, the increases in heat transfer coefficients due to mainstream turbulence (from 0.7% to 17%) are more significant at higher blowing ratios. Farther downstream of the film holes on the pressure surface, heat transfer coefficients for any given mainstream turbulence intensity are almost independent of blowing ratio, which indicates that the mainstream turbulence generated boundary layer disturbance is stronger than the injectant jet generated one and also indicates film dilution. On the pressure surface, both density ratio injectants show the same levels of heat transfer coefficients at the lowest blowing ratio of 0.4, because the amounts of injectant coming out and their momentum flux ratios are very small; whereas, at higher blowing ratios, the density ratio effect becomes more significant near the film injection locations, with the low density ratio injectant (air) producing higher heat transfer coefficients for the reason explained before (Fig. 4). At further downstream locations on the pressure surface, the density ratio effect on heat transfer coefficients is very small due to film dilution.

The effect of mainstream turbulence on spanwise-averaged film effectiveness distribution for air and CO_2 injections at the blowing ratios of 0.4, 0.8 and 1.2 is shown in Figs. 6, 7 and 8, respectively. The effect of mainstream turbulence, in addition to the film injec-

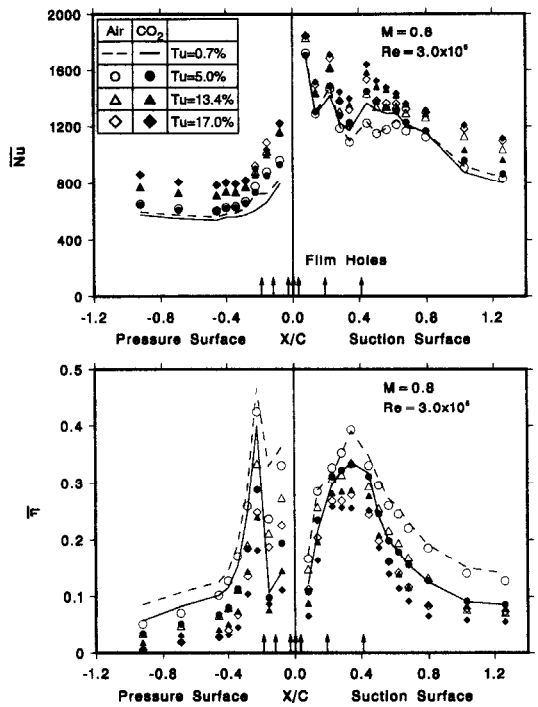

FIG. 7. Effect of mainstream turbulence and air or CO_2 injection on $\overline{Nu}$ and $\bar{\eta}$ distributions for $M = 0.8$.

tion effect is shown in these figures. As mainstream turbulence increases, flow fluctuations disrupt film coverage which results in lower film effectiveness values. For CO_2 and air injections, the decreases in film effectiveness (from the no-grid case) due to mainstream turbulence are more significant at blowing ratio of 1.2 and 0.8, respectively. Since the blowing ratio of 1.2 provides the best film coverage for CO_2 injection under the no-grid condition, any boundary layer disturbance results in much lower film effectiveness values. For the same reason, the effect of mainstream turbulence on film effectiveness is more significant at the blowing ratio of 0.8 for air injection. On the suction surface, CO_2 injection provides higher film efffectiveness than air injection at the blowing ratio of 1.2; however, the effect is reversed at the blowing ratio of 0.4. Because CO_2 provides optimum film coverage at the blowing ratio of 1.2, and since the momentum flux ratio for air injection at that blowing ratio is very high, the above-mentioned effect is observed. At the low blowing ratio of 0.4, the injection jet for CO_2 injection has a very small momentum flux ratio making the jet very weak. Hence, air injection at the blowing ratio of 0.4 provides higher film effectiveness values than CO_2 injection. This is consistent with the observations of Ito *et al.* [18] and Haas *et al.* [19].

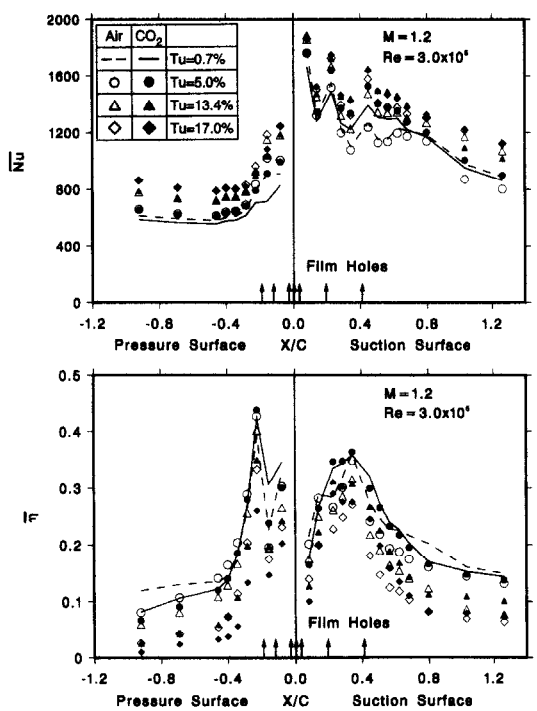

FIG. 8. Effect of mainstream turbulence and air or CO_2 injection on $\overline{Nu}$ and $\bar{\eta}$ distributions for $M = 1.2$.

CONCLUDING REMARKS

The effect of grid-generated mainstream turbulence on film effectiveness and heat transfer coefficient distributions of a model turbine blade, with air (DR $\approx$ 1.0) or CO_2 (DR $\approx$ 1.5) film injection, in a linear cascade was investigated. Tests were performed at the chord Reynolds number of 3×10^5, at mainstream turbulence intensities of 0.7%, 5%, 13.4% and 17%, and at blowing ratios of 0.4, 0.8 and 1.2.
The main findings are:

(1) Mainstream turbulence by itself, i.e. for the no-film-holes case, promotes an earlier boundary layer transition and increases the transition length on the suction surface. Heat transfer coefficients on the entire blade surface increase with increasing mainstream turbulence. These increases over the 'no-grid no-film-holes' data are much higher on the suction surface (up to 239%) as compared to those on the pressure surface (up to 101%). Thus, by itself, mainstream turbulence has a very dominant effect on heat transfer coefficients.
(2) Film holes by themselves, i.e. without film injection, produce high heat transfer coefficients on the suction surface that are comparable with the 'strongest turbulence ($Tu = 17\%$) and no-film-holes' case.
(3) Film injection by itself, i.e. for the no-grid case, produces even higher heat transfer coefficients on most of the suction surface. Over most of the surface (up to 80% chord length), heat transfer coefficients for the 'no-grid and film injection' case are much higher than for the 'strongest turbulence ($Tu = 17\%$) and no-film-holes' case. Thus, on the suction surface, film injection by itself has an even

more dominant effect on heat transfer coefficients than grid turbulence by itself.

(4) When mainstream turbulence is imposed on top of film injection, the effect is a further increase in heat transfer coefficients over the entire test surface. As blowing ratio increases, the increases in heat transfer coefficients due to mainstream turbulence reduce, except in the suction surface accumulation region where they increase. On most of the suction surface (up to 80% chord length), however, the effect of mainstream turbulence in addition to film injection is secondary when compared with only the film injection effect.

(5) In general, as blowing ratio increases, surface heat transfer coefficients increase. On most of the suction surface (up to 80% chord length), however, the effect of blowing ratio is secondary when compared with only the film-injection effect.

(6) For the no-grid case, blowing ratios of 1.2 and 0.8 provide the best film effectiveness over most of the blade surface for CO_2 and air injections, respectively.

(7) When the mainstream turbulence condition is imposed on top of film injection, the effect is a decrease in film effectiveness values over most of the blade surface for both density ratio injectants and at all blowing ratios, the decreases being more significant at blowing ratios of 1.2 and 0.8 for CO_2 and air injections, respectively.

(8) When mainstream turbulence is imposed on top of film injection, CO_2 injection provides better film effectiveness than air injection at the highest blowing ratio of 1.2, whereas the effect is reversed at the lowest blowing ratio of 0.4.

The effect of several important parameters (mainstream turbulence, density ratio, and blowing ratio) on heat transfer coefficient and film effectiveness distributions for a turbine blade model with film injection has been presented in this paper. The paper also indicates the relative strengths of these parameters. These results can be used in gas turbine blade design.

Acknowledgements—The project was sponsored by the Texas Higher Education Coordinating Board—Advanced Technology Program under grant number 999903-104 and by the U.S. Naval Air Warfare Center through General Electric Aircraft Engines.

REFERENCES

1. R. J. Goldstein, Film cooling. In *Advances in Heat Transfer*, Vol. 7 (Edited by T. F. Irvine, Jr. and J. P. Hartnett), pp. 321–379. Academic Press, New York (1971).
2. J. C. Han and A. B. Mehendale, Flat plate film cooling with steam injection through one row and two rows of inclined holes, *ASME J. Turbomachinery* **108,** 137–144 (1986).
3. S. G. Schwarz, R. J. Goldstein and E. R. G. Eckert, The influence of curvature on film cooling performance, *ASME J. Turbomachinery* **113,** 472–478 (1991).
4. W. J. Mick and R. E. Mayle, Stagnation film cooling and heat transfer, including its effect within the hole pattern, *ASME J. Turbomachinery* **110,** 66–72 (1988).
5. A. B. Mehendale and J. C. Han, Influence of high mainstream turbulence on leading edge film cooling heat transfer, *ASME J. Turbomachinery* **114,** 707–715 (1992).
6. A. B. Mehendale and J. C. Han, Influence of high mainstream turbulence on leading edge film cooling heat transfer: effect of film hole spacing, *Int. J. Heat Mass Transfer* **35,** 2593–2604 (1992).
7. R. J. Goldstein, E. R. G. Eckert and F. Burggraf, Effects of hole geometry and density on three-dimensional film cooling, *Int. J. Heat Mass Transfer* **17,** 595–605 (1974).
8. D. R. Pedersen, E. R. G. Eckert and R. J. Goldstein, Film cooling with large density differences between the mainstream and the secondary fluid measured by the heat-mass transfer analogy, *ASME J. Heat Transfer* **99,** 620–627 (1977).
9. A. K. Sinha, D. G. Bogard and M. E. Crawford, Film-cooling effectiveness downstream of a single row of holes with variable density ratio, *ASME J. Turbomachinery* **113,** 442–449 (1991).
10. A. J. H. Teekaram, C. J. P. Forth and T. V. Jones, The use of foreign gas to simulate the effect of density ratios in film cooling, *ASME J. Turbomachinery* **111,** 57–62 (1989).
11. R. S. Abhari and A. H. Epstein, An experimental study of film cooling in a rotating transonic turbine, ASME Paper No. 92-GT-201 (1992).
12. K. Takeishi, S. Aoki, T. Sato and K. Tsukagoshi, Film cooling on a gas turbine rotor blade, *ASME J. Turbomachinery* **114,** 828–834 (1992).
13. S. Ou, J. C. Han, A. B. Mehendale and C. P. Lee, Unsteady wake over a linear turbine blade cascade with air and CO_2 film injection: part I—effect on heat transfer coefficients, to appear in *ASME J. Turbomachinery*, ASME Paper No. 93-GT-210 (1993).
14. A. B. Mehendale, J. C. Han, S. Ou and C. P. Lee, Unsteady wake over a linear turbine blade cascade with air and CO_2 film injection: part II—effect on film effectiveness and heat transfer distributions, to appear in *ASME J. Turbomachinery*, ASME Paper No. 93-GT-134 (1993).
15. J. C. Han, L. Zhang and S. Ou, Influence of unsteady wake on heat transfer coefficient from a gas turbine blade, *ASME J. Heat Transfer* **115,** 904–911 (1993).
16. S. J. Kline and F. A. McClintock, Describing uncertainties in single-sample experiments, *Mech. Engng* **75,** 3–8 (1953).
17. R. E. Mayle, The role of laminar–turbulent transition in gas turbine engines, *ASME J. Turbomachinery* **113,** 509–537 (1991).
18. S. Ito, R. J. Goldstein and E. R. G. Eckert, Film cooling of a gas turbine blade, *ASME J. Engng Power* **100,** 476–481 (1978).
19. W. Haas, W. Rodi and B. Schönung, The influence of density difference between hot and coolant gas on film cooling by a row of holes: predictions and experiments, *ASME J. Turbomachinery* **114,** 747–755 (1992).